Received: 2 June 2020 | Revised: 24 July 2020 | Accepted: 26 August 2020

DOI: 10.1002/tbio.202000014

FULL ARTICLE

TRANSLATIONAL BIOPHOTONICS

Prediction of pathological response to neo-adjuvant chemoradiotherapy for oesophageal cancer using vibrational spectroscopy

Thi N. Q. Nguyen[1,2] | **Adrian Maguire**[1] | **Catherine Mooney**[3] | **Naomi Jackson**[1] | **Niamh Lynam-Lennon**[5] | **Vicki Weldon**[1,2] | **Cian Muldoon**[4] | **Aoife A. Maguire**[4] | **D. O'Toole**[4] | **Narayanasamy Ravi**[5] | **John V. Reynolds**[5] | **Jacintha O'Sullivan**[5] | **Aidan D. Meade**[1,2]

[1]Centre for Radiation and Environmental Science, Focas Research Institute, Technological University Dublin, Dublin, Ireland

[2]School of Physics and Clinical and Optometric Sciences, Technological University Dublin, Dublin, Ireland

[3]School of Computer Science, University College Dublin, Dublin, Ireland

[4]Department of Histopathology, St. James's Hospital, Dublin, Ireland

[5]Trinity Translational Medicine Institute, Department of Surgery, Trinity College Dublin, St James's Hospital, Dublin, Ireland

Correspondence
Dr Aidan D. Meade, School of Physics and Clinical and Optometric Sciences, TU Dublin, City Campus, Dublin 8, Ireland.
Email: aidan.meade@tudublin.ie

Funding information
Health Research Board, Grant/Award Number: HRA-POR-1314-2015; Science Foundation Ireland, Grant/Award Numbers: 12/TIDA/B2406, 13/RC/2106

Abstract

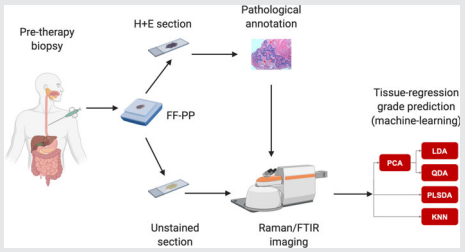

In oesophageal cancer (OC) neo-adjuvant chemoradiotherapy (neoCRT) is used to debulk tumour size prior to surgery, with a complete pathological response (pCR) observed in approximately ~30% of patients. Presently no predictive quantitative methodology exists which can predict response, in particular a pCR or major response (MR), in patients prior to therapy.

Raman and Fourier transform infrared imaging were performed on OC tissue specimens acquired from 50 patients prior to therapy, to develop a computational model linking spectral data to treatment outcome. Modelling sensitivities and specificities above 85% were achieved using this approach. Parallel in-vitro studies using an isogenic model of radioresistant OC supplied further insight into OC cell spectral response to ionising radiation where a potential spectral biomarker of radioresistance was observed at 977 cm^{-1}.

This work demonstrates that chemical imaging may provide an option for triage of patients prior to neoCRT treatment allowing more precise prescription of treatment.

Abbreviations: CRM, confocal Raman microspectroscopy; FTIR, Fourier Transform Infrared; LDA, Linear discriminant analysis; neoCRT, neo-adjuvant chemoradiotherapy; OC, oesophageal cancer; PCA, Principal components analysis; pCR, complete pathological response; PLSDA, Partial least squares discriminant analysis; ROC AUC, receiver-operator-characteristic area-under-the-curve; TMA, tissue-micro-array; TRG, Tissue regression grade.

[Correction added on 15 October 2020, after first online publication: "Vicki Weldon" has been added as a co-author in this version of the article.]

KEYWORDS

complete pathological response, FTIR spectroscopy, machine learning, neo-adjuvant chemoradiotherapy, Raman spectroscopy

1 | INTRODUCTION

Oesophageal cancer (OC) presents a significant therapeutic challenge to cure. There are two main disease subtypes: oesophageal adenocarcinoma (OAC; originating in glandular cells) and squamous cell carcinoma (SCC; originating in squamous epithelial cells). Today almost half of the worldwide OAC burden occurs in Western Europe, America and Oceania.[1] For instance over the period from 1972 to 2012 the incidence rate trebled in both males and females in the UK[2], and rapid rises in incidence are predicted to occur in the EU from the present beyond 2030.[1,3]

In patients who present with locally advanced disease and are considered for treatment with curative intent, current therapeutic regimens focus on neo-adjuvant treatment (prior to surgery) with chemotherapy alone or neo-adjuvant chemoradiotherapy (neoCRT). Randomised clinical trials (RCTs) have established that these combination treatments significantly improve cure rates compared with surgery alone,.[4–6] At this time approximately 30% of patients undergoing neoCRT prior to resection will have no evidence of cancer in the resection specimen, a so-called complete pathological response (pCR). If this response could be predicted prior to treatment such patients may possibly be spared surgery. Conversely, for patients who are resistant to treatment, and may possibly be harmed by a long delay to surgery, this information may completely alter the treatment pathway.

While it was hoped that genomic methods could permit prediction of response[7–10] in their totality investigations in this domain have had limited success owing to challenges surrounding study design, power[11–13] and in particular the complexity of tumour heterogeneity. Biophotonic imaging technologies (via Raman or Fourier-transform infrared [FTIR] spectroscopy) have demonstrated application to the objective classification of tissue histopathology ex-vivo[14] or in-situ,[15] with the identification of disease biomarkers in tissue[16–19] and biofluids.[20,21] Critically, recent results have also suggested the existence of spectral biomarkers of radio- and chemotherapeutic response[22–25] that are capable of discriminating patients by response both before and during treatment.[26,27]

The objective of this study was to investigate whether the spectral fingerprints of OC tissue, obtained via confocal Raman spectra and FTIR spectra, could be used to predict neoCRT response prior to treatment. Tumour regression grade (TRG) represents a pathological measure of neoCRT response using a 5-point scale where a TRG 1 represents complete regression, 2 represents a partial regression, 3 is an intermediate regression and 4 and 5 represent slight to no regression.[28] In patients, tissue spectra were recorded using both modalities, and after post-processing of spectral measurements, classification models for TRG were constructed using various machine learning approaches, with particularly encouraging classification performance seen with partial-least-squares discriminant analysis (PLSDA).

Additionally spectral profiles of an isogenic cell line model of radioresistant OC (OE33 cell line) were used to elucidate spectral biomarkers that could identify profiles of radioresistance for reference to tissue spectra in patients with poor neoCRT response. The primary parental OE33 line (OE33P) was originally established from OAC with a radioresistant subline (OE33R) generated by exposing the OE33 parental line to 50Gy of fractionated X-radiation (2Gy per fraction).[29] This isogenic model has been previously used to elucidate molecular markers underlying radioresistance in OC and has revealed the interlinking roles played by DNA repair efficiency, ROS damage of mitochondria and altered energy metabolism associated with this radioresistant phenotype.[30,31] In the present instance spectra of this line were studied with the purpose of establishing and explaining Raman spectral biomarkers of radioresistance that could correlate with observations in patient tissue. Although a potential spectral biomarker was found at 977 cm^{-1} in the cell line model a corresponding feature was not observed in tissue and therefore this observation requires further validation.

This proof-of-concept study may be encouraging for the future deployment of spectroscopic technologies as a pre-therapeutic predictive triage for OC patients.

2 | MATERIALS AND METHODS/ EXPERIMENTAL

2.1 | Cell lines

The human OAC cell line OE33 was obtained from the European collection of cell cultures. OE33 P (radio-sensitive) and OE33 R (radio-resistant) cells were generated, cultured and characterised in our laboratory as previously described.[29]

2.2 | Cell irradiation

In-vitro cultured OE33R and OE33P cells were irradiated in triplicate with 2Gy (or sham-irradiated) using a Gulmay Medical X-ray generator (RS225, Gulmay Medical). The dose rate at the sample was 1.5 Gy/min and the photon energy was 200 kV. Cells were fixed at 24 hours post-irradiation using 4% paraformaldehyde in dH_2O, and were drop cast onto calcium fluoride slides (CaF_2; Crystran Ltd., UK). Cells were air dried and stored in a desiccator until the time of spectral analysis.

2.3 | Tissue characteristics and ethical considerations

Following ethical approval (Joint St James's Hospital/Tallaght University Hospital joint Research Ethics Committee) and written informed consent, diagnostic biopsy specimens were taken from patients with a diagnosis of operable OC, by a qualified endoscopist (D.O'T, N.R.) prior to neo-adjuvant therapy. The tissue was preserved in a standard manner through fixation in 4% formalin solution and subsequently embedded in paraffin wax. Histologic confirmation of tumour tissue in biopsies was performed by a pathologist using routine haematoxylin and eosin staining.

Patients received a complete course of neoCRT. Surgical resection was performed within 1 month of completing the CRT regimen. All resected esophagectomy specimens were assessed by a consultant GI pathologist (C.M.). Tumour pathological response to treatment was assigned a TRG score between 1 and 5, as previously described.[28]

A 10 μm thick section was cut from each full face tissue block using a microtome and the tissue was mounted on a 2.5 mm thick calcium fluoride (CaF_2) slide for vibrational spectroscopy. A parallel 4 μm thick section was also cut a stained with haemotoxylin & eosin (H + E) for reference purposes during spectroscopic histopathological imaging. The tissue for spectroscopic imaging was subsequently chemically dewaxed according to a protocol described elsewhere.[32]

In addition, a tissue-micro-array (TMA) was prepared from full face biopsy specimens, as described previously.[30] Tissue cores with a diameter of 0.6 mm were taken using a precision instrument (Beechers Inc.), and a TMA block prepared. A single 10 μm section of this block was prepared for spectroscopic analysis with chemical dewaxation as noted earlier here. This cohort contained both OAC and SCC tissues. Both were incorporated within the study. Patient cohort characteristics are outlined in Table 1.

TABLE 1 Patient cohort characteristics

	Gross sections	TMA
Patients *(n)*	31	19
Male	27	16
Female	4	3
Age (Years)*	60 (37-76)	62 (45-75)
Histology		
Adenocarcinoma	31	15
Squamous cell carcinoma	0	4
Clinical TNM stage		
0	0	0
I	0	0
IIa	18	11
IIb	1	1
III	12	7
IV	0	0
Clinical nodal status		
N0	17	10
N1	14	9
TRG		
1	6	2
2	11	3
3	10	8
4	4	4
5	0	2

Abbreviations: N0, lymph node metastasis negative; N1, lymph node metastasis positive TMA, tissue-microarray; TNM, tumour-node-metastasis; TRG, tumour regression grade.
*Values given are mean (range).

In total, OC tissues from 50 patients who had provided their full consent were used in this work. The acquisition of both FTIR and Raman spectra was guided by contiguous H&E stained sections of each tissue sample. A typical H + E stained section is shown in Figure 1, with epithelia and stroma highlighted.

2.4 | Spectroscopic measurements

2.4.1 | Raman spectroscopy

For measurements on cultured cells, Raman spectroscopy was performed using a Horiba Jobin Yvon Labram HR800 UV spectrometer. Spectra were acquired with a 532 nm solid-state diode laser delivering 100 mW of power to the sample through a ×100 objective (NA = 0.9), over a 6 second integration time with individual spectra

averaged across three integrations. In the case of the cellular samples, approximately 150 to 160 point spectra were acquired from the nuclear portion of 60 cells for each triplicate sample at each dose, giving rise to a dataset of approximately 1900 spectra for final analysis.

Similarly for measurements on OC tissue, Raman spectroscopy was performed with the same system using a 660 nm solid-state diode laser delivering 100 mW of power to the sample. Each individual tissue spectrum was measured with a 20 second integration time averaged across three integrations. Spectral measurements were performed separately on epithelia and stromal portions of the tissue. A total of 100 spectra were recorded separately from both the stroma and epithelial portions of the tissue from each patient using the parallel H + E stained section as a guide.

For all spectra wavenumber calibration in post-processing was conducted using a spectrum of 1,4-bis(2-methyl-styryl) benzene as a reference, which was acquired at the time of analysis of all biological samples. A diffraction grating ruled with 300 lines per mm was used for spectral dispersion in each case, resulting in a spectral resolution of ~2.1 cm^{-1}. In recording spectra, the confocal hole was set to 100 μm with the grating centred at 1350 cm^{-1}.

2.4.2 | FTIR spectroscopic measurements

FTIR images were acquired in transmission mode using a Spectrum Spotlight 400 FTIR imaging system (Perkin Elmer, Dublin, Ireland; NA = 0.6), equipped with a liquid nitrogen-cooled mercury cadmium telluride detector in transmission mode. Each image was recorded with a pixel size of 6.25 μm^2, with a 4 cm^{-1} spectral resolution and averaged over 128 scans in the range from 750 cm^{-1} to 4000 cm^{-1}.

Spectra were corrected for atmospheric interference from CO_2 and water vapour using routines within the SpectrumIMAGE software (PerkinElmer), and were converted from transmittance to absorbance for analysis.

2.5 | Spectral data pre-processing

Raman and IR spectra were next pre-processed using in-house code developed within Matlab R2017a (Mathworks) which utilised methods within PLS-Toolbox version 8.02 (Eigenvector Research Inc.).

For Raman spectra of OE33 cells, OC epithelia and stroma the pre-processing steps included: wavenumber calibration, baseline correction, smoothing (with a Satvitzsky-Golay filter, fifth-order polynomial and 15-point window) and vector normalisation as detailed in previous work.[33] Approximately 6800 spectra were retained for further analysis.

IR spectra from all tissue subcomponents were pooled, limited to the fingerprint region (1000-1800 cm^{-1}) and corrected using the resonant Mie-extended multiplicative scattering correction (RMie-EMSC).[34] The corrected spectra were next subjected to outlier removal, vector normalisation and inter-sample averaging[23] (within each patient image) in order to provide a reduced spectral set of ~190 000 spectra for analysis.

2.6 | Spectral data analysis and classification of TRG scores

Each of the following spectral analysis methods were implemented in Matlab R2017a (Mathworks), aside from the exploratory PCA analysis of the spectral data from the OE33 cell line which was implemented in Python 3.7.

2.6.1 | Principal component analysis

Principal component analysis (PCA)[35] is a commonly used unsupervised method that reduces dimensionality and transforms a spectral dataset of N wavenumbers to a set of linearly uncorrelated M variables (where $M<N$) while retaining most of the signal within the original dataset. These linearly uncorrelated variables are termed principal components (PCs). Each PC describes a proportion of the variance of the original dataset in a decreasing fashion, where each PC is also orthogonal to all other PCs. Here PCA was performed with mean-centering.

2.6.2 | TRG classification under bootstrap strategy

Separate models for prediction of TRG score were constructed using Raman and FTIR spectra, respectively, using an approach described previously[26] incorporating some modifications. Here, owing to the small sample size, all classification models were constructed and optimised using 0.632 bootstrapping. Model performance was measured as the area under the curve of the receiver operator characteristic (ROC AUC). Models were repeatedly evaluated on randomly sorted data to define tolerances on ROC AUC figures. The modelling schema is presented in Figure 2, using modelling algorithms including PCA-linear discriminant analysis (LDA), PCA-quadratic discriminant analysis (QDA), Partial least squares-discriminant analysis (PLSDA) and K-nearest neighbours (KNN).

K-nearest neighbours

KNN[36,37] is a non-parametric method of classification, which is widely employed in machine learning. To classify an unknown sample, KNN classification starts by calculating the distance of that sample to all the samples of the training dataset. The most represented class from the k smallest distances is thus the class label of the unknown sample. Here prototype KNN classifiers were optimised by varying the value of k from 1 to 50.

PCA-linear discriminant analysis

LDA[38] is a binary classification method. LDA assumes that data from each class is distributed normally with equal covariance in each class, and uses the Bayes Theorem to estimate a linear boundary that optimally separates the data of each class. Here LDA models used PC scores of spectra as input (PCA-LDA). To optimise and evaluate model performance, PCA-LDA was run with a number of PCs varying from 1 to 50.

PCA-quadratic discriminant analysis

Closely related to LDA, QDA[38] is also a binary classification method based on the Bayes Theorem. Again it is assumed that each class is normally distributed, though no assumption is made regarding the equality of the covariance matrices. This leads to the decision boundary being quadratic in shape. Again, coupled with PCA, PCA-LDA was optimised by evaluating its performance while varying the number of PCs from 1 to 50.

Partial least squares-discriminant analysis

PLSDA[39] is a supervised multivariate classification method that is widely used with spectral datasets.[40] Similar to PCA, PLSDA can be employed as a feature extraction method though in contrast to PCA PLSDA it aims to reduce dimensionality by transforming a spectral dataset of N wavenumbers to a set of M linear features (where $M<N$), while preserving as much covariance as possible between the dataset and its corresponding response

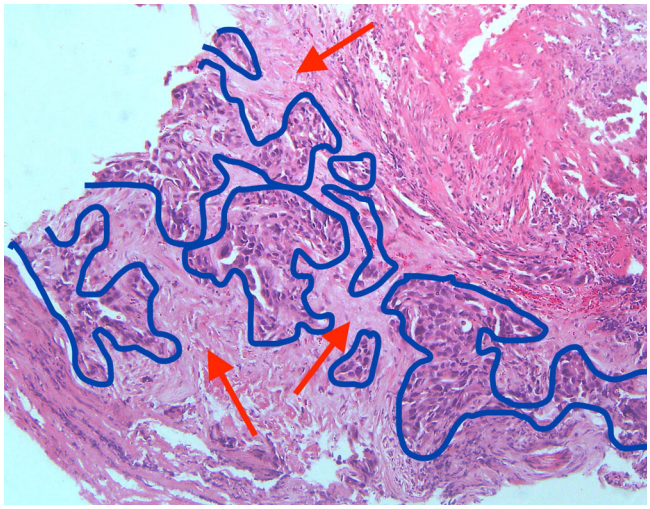

FIGURE 1 Typical haemotoxylin-eosin stained section of oesophageal adenocarcinoma used as a reference for spectroscopic imaging. Epithelial cells are identified by a blue border, while red arrows identify the location of surrounding stroma

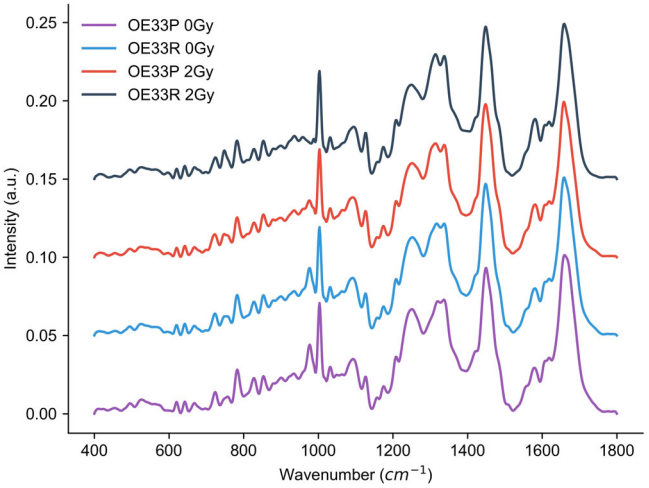

FIGURE 3 Mean spectra of OE33 P and R isogenic cell line model with irradiation condition. A distinct band centred at 977 cm^{-1} is diminished after 2Gy irradiation in both the parental (P) and resistant (R) lines

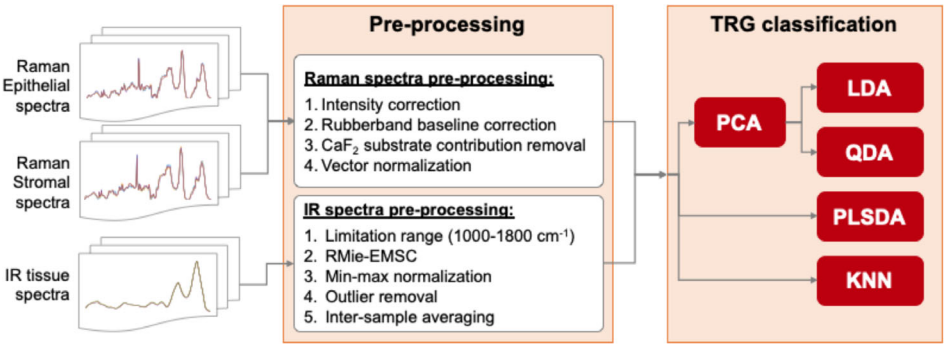

FIGURE 2 Flowchart depicting the preprocessing and TRG-score classification pipelines for Raman and FTIR spectra. Several machine learning methods have been used for TRG classification in order to define an optimal classification model (TRG is tissue regression grade)

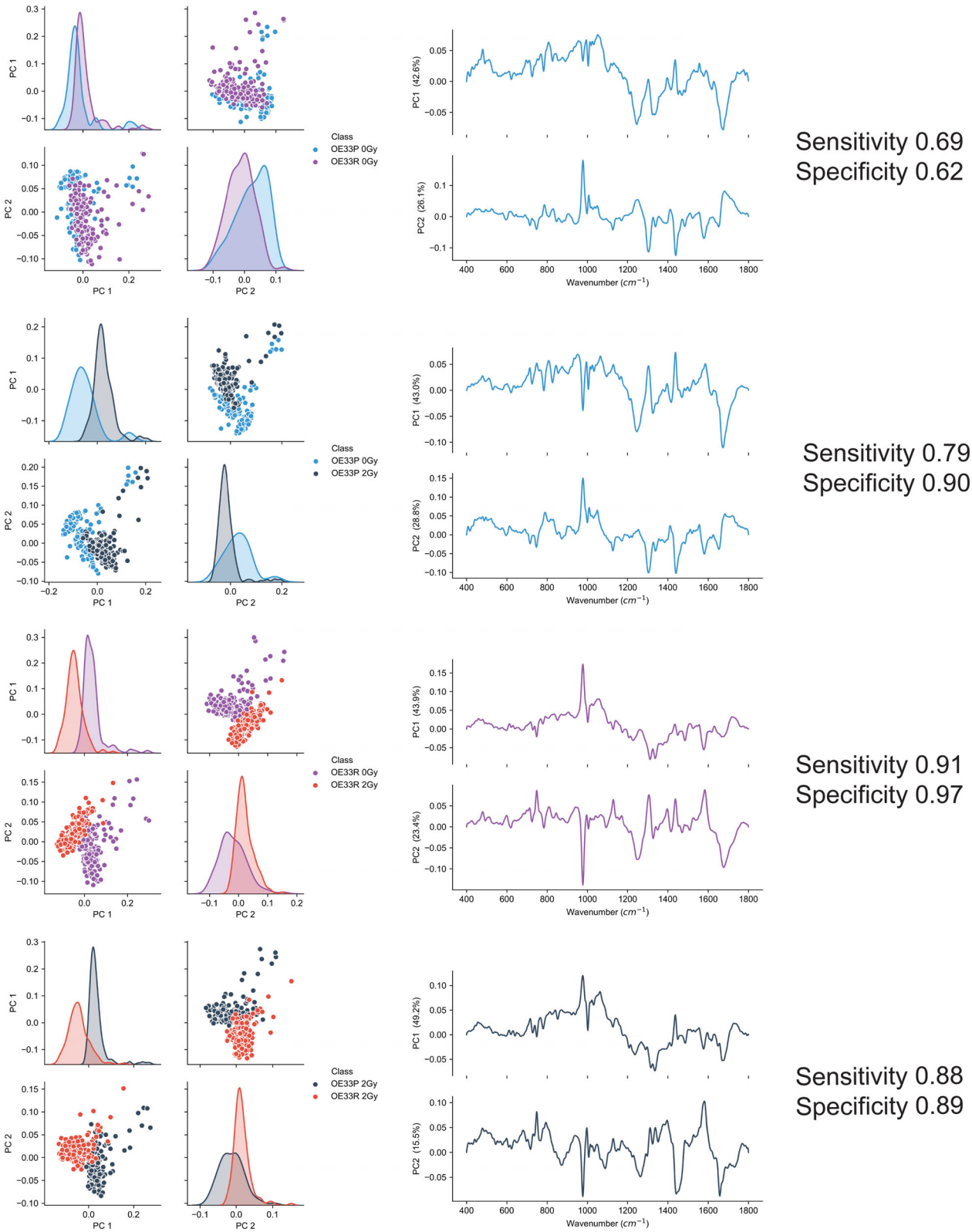

FIGURE 4 PCA of OE33 isogenic cell line model with irradiation condition. Sensitivities and specificities of classification using an LDA model are included for each pairwise classification. Spectral discriminants (loadings in righthand panels) are dominated by mode centred at 977 cm^{-1}, especially in discriminating irradiated resistant (R) and parental (P) lines and in discriminating resistant control (0Gy) form its irradiated counterpart. LDA, linear discriminant analysis; PCA, principal components analysis

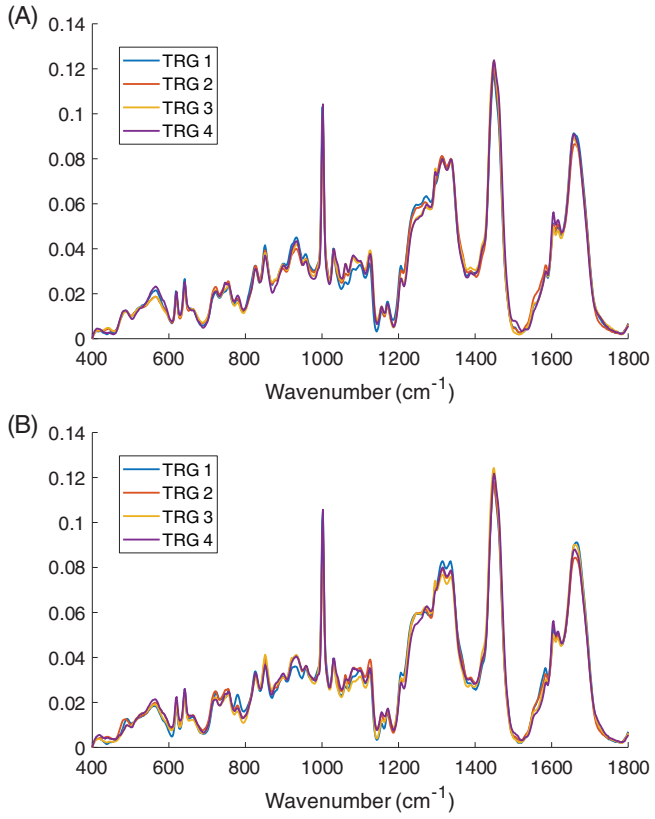

FIGURE 5 Mean Raman spectra of OC tissue by TRG score for A, epithelia and B, stroma. OC, oesophageal cancer; TRG, tissue regression grade

variable (the class label). The linear features are termed latent variables (LVs) to distinguish them from PCs, and in contrast to PCA each LV is not orthogonal to the others within the model. In the present instance the PLSDA model complexity was optimised by varying the number of LVs from 1 to 50.

Bootstrap strategy

In order to obtain a robust estimate of classifier performance, a bootstrap cross-validation strategy[42] was employed. Bootstrapping aims to generate b new datasets for the development of b classification models. Firstly, a set of test data is randomly selected (the "out-of-bag" samples). Then the remaining data is used to construct a set of bootstrapped training sets by randomly drawing samples n times with replacement, where n is the number of spectra within the original dataset. The final bootstrap classification performance (CP) is thus averaged over the number, b, of bootstrapped datasets.

To circumvent the pessimistic bias[43] in bootstrap cross-validation, the CP in this study was calculated using the .632 estimate approach[43] as below:

$$\mathrm{CP}_{boot} = \frac{1}{b}\sum_{i=1}^{b}(0.632\,\mathrm{CP}_{oob}(i) + 0.368\,\mathrm{CP}_{r}(i)),$$

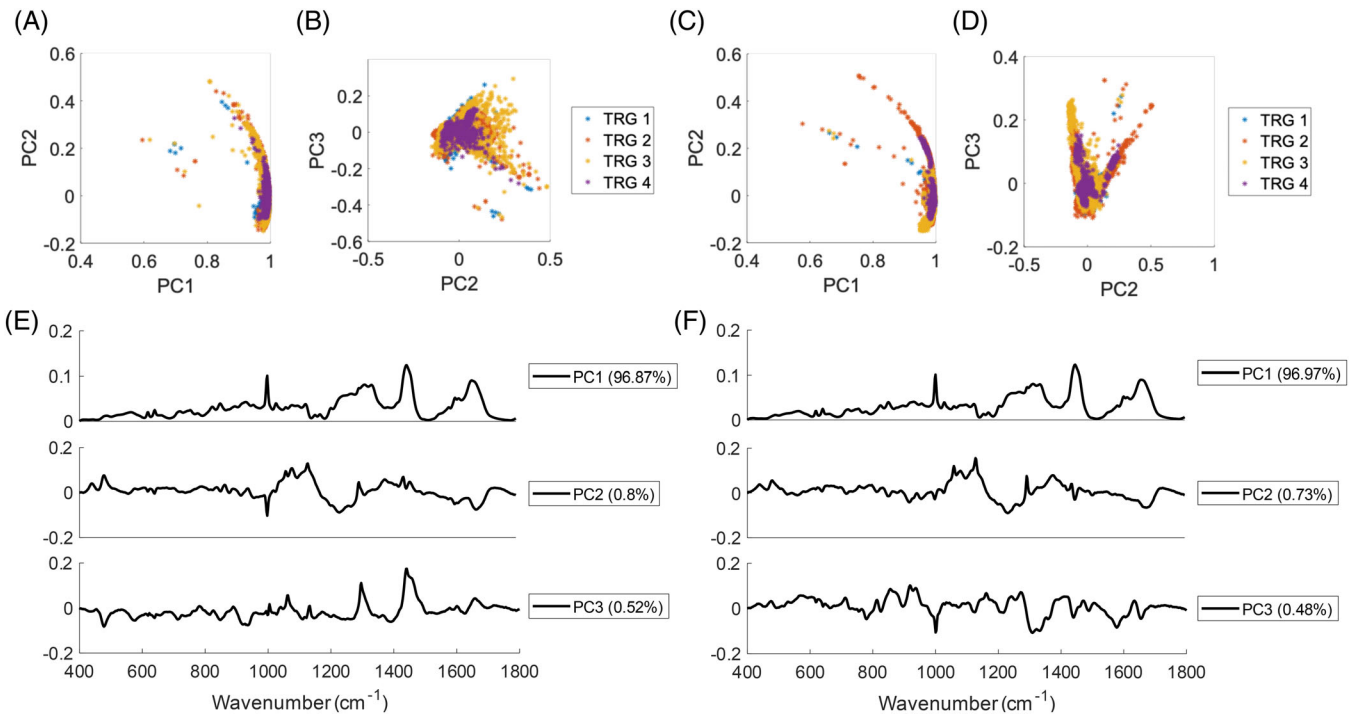

FIGURE 6 Visualisation of PCA applied to Raman spectra of OC tissue. In A, B, and C scores and loadings for analysis of epithelia are shown, with scores and loadings for stroma in D, E, and F. No clear discrimination by TRG class is observed between the scores of the first three components for either tissue structure. OC, oesophageal cancer; PCA, principal components analysis; TRG, tissue regression grade

where, at the i[th] bootstrap dataset, $CP_{oob}(i)$ is the classification performance on the out-of-bag test sample, and $CP_r(i)$ is the resubstitution classification performance calculated using the bootstrap training set.

As recommended in previous work,[42] b was set to 100. The out-of-bag test set was constructed by randomly extracting 40% of patient spectra (with stratified sampling by class) and the remaining spectral dataset was used for the generation of bootstrap training sets. This bootstrapping procedure was used to select the optimal number of PCs for PCA-LDA/QDA, the optimal number of LVs for PLSDA and the value of k for KNN.

The classification performance of each fitted model was measured as the classification accuracy, the F1-score and ROC AUC. The optimal model for each algorithm was taken as that which gave the highest ROC AUC.

As a final validation check to ensure model overfitting did not occur, a methodology suggested by Westerhuis[41] was employed, whereby separate models were constructed in which the class label for each spectrum was randomly assigned at training and the model performance was evaluated. A sample of this result is depicted in Figure S2.

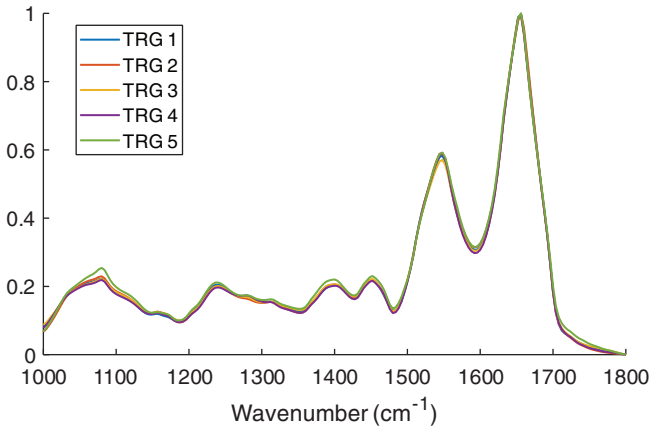

FIGURE 7 Mean fingerprint FTIR spectra of OC tissue by TRG score. FTIR, Fourier transform infrared; OC, oesophageal cancer; TRG, tissue regression grade

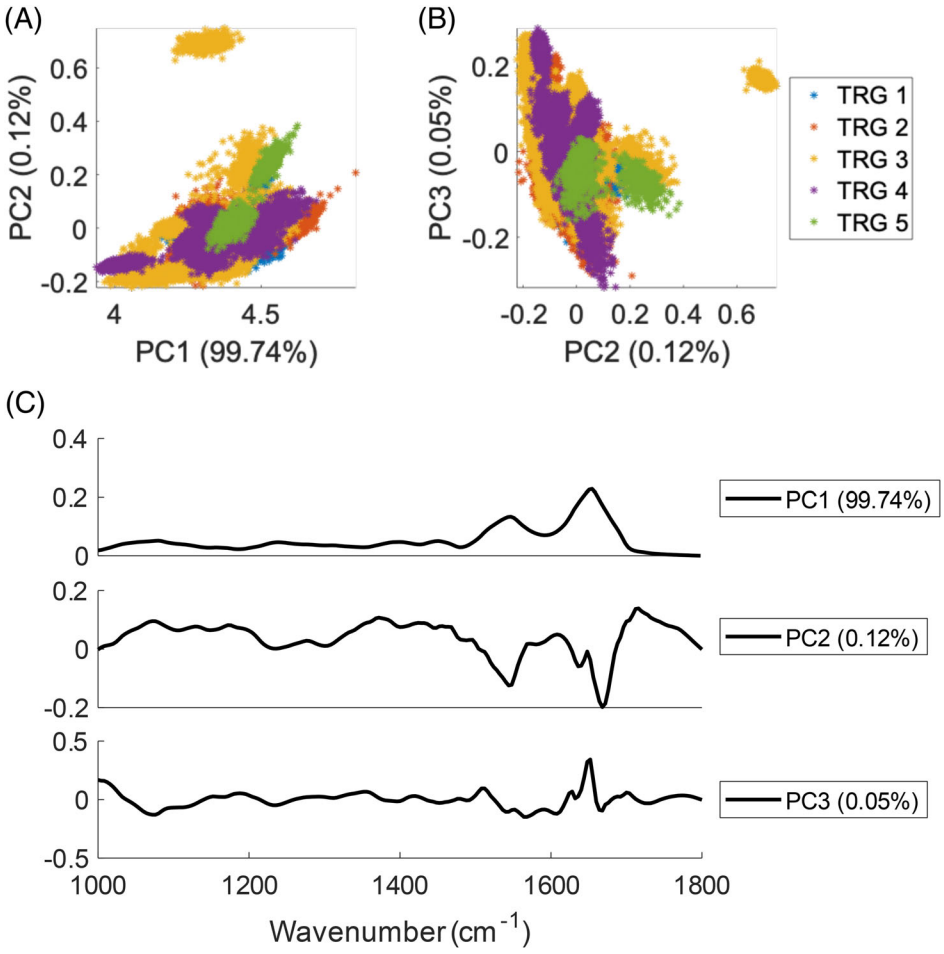

FIGURE 8 Visualisation of PCA applied to FTIR spectra of OC tissue. In A, and B, scores are plot, while in C, loadings are shown. No clear discrimination by TRG class is observed between the scores of the first three components. FTIR, Fourier transform infrared; OC, oesophageal cancer; PCA, principal components analysis; TRG, tissue regression grade

TABLE 2 Optimal oesophageal cancer TRG classification performance, estimated by .632 bootstrap cross-validation, using Raman spectra of epithelium and stroma tissue structure

		Epithelia				Stroma			
	Classifier	AUC (%)	Median (comp)	IQR (comp.)	Accuracy (%)	AUC (%)	Median (comp)	IQR (comp.)	Accuracy (%)
TRG 1 vs 2–3-4	KNN	78 ± 4	1	0	81 ± 4	81 ± 4	1	29	82 ± 5
	PLSDA	68 ± 8	7	15	79 ± 6	73 ± 7	3	4	64 ± 8
	PCA-LDA	69 ± 10	15	19	77 ± 6	70 ± 10	11	17	66 ± 7
	PCA-QDA	82 ± 8	29	24	87 ± 3	85 ± 6	12	15	82 ± 4
TRG 1–2 vs 3-4	KNN	71 ± 6	1	0	63 ± 6	72 ± 5	1	0	65 ± 5
	PLSDA	65 ± 6	5	10	61 ± 4	64 ± 7	4	8	61 ± 6
	PCA-LDA	66 ± 8	16	19	64 ± 6	66 ± 8	19	17	64 ± 6
	PCA-QDA	64 ± 8	17	29	63 ± 5	69 ± 7	34	22	66 ± 5
TRG 1–2-3 vs 4	KNN	81 ± 3	1	0	88 ± 3	81 ± 4	1	0	85 ± 4
	PLSDA	74 ± 8	9	21	86 ± 4	75 ± 8	15	24	85 ± 5
	PCA-LDA	76 ± 12	18	9	82 ± 6	75 ± 11	27	27	87 ± 4
	PCA-QDA	81 ± 6	23	16	90 ± 1	77 ± 5	40	32	89 ± 2

Note: Greyed values represent the optimal classification performance model with the highest AUC score. (Comp., complexity of the corresponding classifier, that is, the number of k, LVs, and PCs for KNN, PLSDA, and PCA-LDA/QDA, respectively; IQR, interquartile range on complexity parameter). All data are rounded to the nearest whole number where possible.
Abbreviations:AUC, area-under-the-curve; IQR, interquartile range; KNN, K-nearest neighbours; LDA, linear discriminant analysis; PCA, principal components analysis; PLSDA, partial least squares discriminant analysis; QDA, quadratic discriminant analysis; TRG, tissue regression.

TABLE 3 Optimal oesophageal cancer TRG classification performance, estimated by .632 bootstrap cross-validation, using IR spectra of sample tissue

	Classifier	AUC (%)	Median (comp)	IQR (comp.)	Accuracy (%)
TRG 1 vs 2-3-4-5	KNN	85 ± 5	1	2	85 ± 5
	PLSDA	75 ± 9	27	27	80 ± 6
	PCA-LDA	73 ± 11	26	13	80 ± 7
	PCA-QDA	86 ± 5	23	26	88 ± 2
TRG 1–2 vs 3-4-5	KNN	77 ± 5	1	0	70 ± 5
	PLSDA	70 ± 8	24	23	70 ± 6
	PCA-LDA	71 ± 7	25	8	70 ± 6
	PCA-QDA	75 ± 7	20	19	72 ± 5
TRG 1–2-3 vs 4-5	KNN	76 ± 4	1	0	77 ± 5
	PLSDA	70 ± 9	19	18	78 ± 6
	PCA-LDA	70 ± 9	33	25	78 ± 5
	PCA-QDA	80 ± 6	29	29	85 ± 4

Note: Greyed values represent the optimal classification performance model with the highest AUC score. (Comp., complexity of the corresponding classifier, that is, the number of k, LVs, and PCs for KNN, PLSDA, and PCA-LDA/QDA, respectively; IQR, interquartile range on complexity parameter). All data are rounded to the nearest whole number where possible.
Abbreviations: AUC, area-under-the-curve; IQR, interquartile range; KNN, K-nearest neighbours; LDA, linear discriminant analysis; PCA, principal components analysis; PLSDA, partial least squares discriminant analysis; QDA, quadratic discriminant analysis; TRG, tissue regression.

3 | RESULTS AND DISCUSSION

3.1 | Spectral features varying with radioresistance in the OE33 cell line model

Figure 3 depicts the mean spectra of both the radio-resistant OE33R and radiosensitive isogenic parental OE33 P cell lines after irradiation. A clear band centred at 977 cm^{-1} discriminates the two phenotypes, and decreases in both after irradiation.

Previous studies have suggested that this band is related to stretching of the sulphate linkage (-C-O-S-) in glycoprotein. Candidate radio-protective glycoproteins including clusterin (Apo-J) and proteins from the apolipoprotein-E (Apo-E) family were obtained in their lyophilized pure form (Sigma-Aldrich) and their spectra obtained with a 532 nm excitation. Despite the identification of a strong vibration centred at 977 cm^{-1} in Apo-E4 (see Figure S1 in supplementary material) an ELISA analysis of OE33 P and R cell lysates (using a monoclonal antibody to ApoE4 derived from mice [Cell Signalling #8941]) did not demonstrate expression of this protein. It is therefore not possible at present to account for the origin of this band nor to ascribe it any radioprotective significance.

A PCA analysis of spectra from each of the in-vitro irradiated OE33 P and OE33 R phenotypes is depicted in Figure 4, with the corresponding PCA-LDA classification performances (evaluated using leave-one-out cross validation) for each two-way model. From the score plots (left hand column) it was not possible to discriminate between the OE33 P and OE33 R lines at 0Gy where classification performance is low. However spectra of the irradiated OE33 P and OE33 R lines can both be discriminated from their control class, indicating that a radiation response is detectable in this model. Importantly, however, the irradiated OE33 P and OE33 R lines can be discriminated from each other; this demonstrates that the spectral signature of the radioresistant OE33 R phenotype is distinct from that in the radiosensitive OE33 P cell line. The spectral origin of this discrimination may be determined from the PC coefficients (right hand column), each of which contains a strong loading at 977 cm^{-1}, consistent with the analysis of the mean spectra. The intensity of this peak may then be considered a spectral biomarker of radioresistance in this in-vitro model, though its molecular significance remains unclear.

3.2 | Spectral features varying with OC tumours and their TRG score

As described in the methods section of this article, the acquisition of Raman spectra from OC tissue specimens was guided by a parallel H + E stained section. In Figure 5A,B the mean Raman spectra of epithelia and stroma are presented, with varying TRG score. It must be noted that substantial tissue fluorescence was observed in the study for Raman spectra acquired at 660 nm excitation, such that the spectra from several tissue samples were rendered unsuitable for analysis. This reduced the numbers of full-face tissue specimens that could be employed in the study to 31, in which TRG scores varied from 1 to 4. This difficulty was only experienced with Raman imaging data while FTIR spectra from all 50 patients in the study were retained for analysis, with TRG scores varying from 1 to 5.

In Figure 5A some visually observable spectral differences in spectra of epithelia as they vary with TRG score are located at (a) 504 to 612, (b) 708 to 792, (c) 899 to 979, (d) 1200 to 1282, (e) 1296 and (f) 1523 to 1592 cm^{-1}. Similarly, differences between the mean Raman spectra of stroma at each TRG grade (Figure 5B) were observed at 504 to 612, 708 to 792, 868 to 985, 1070 to 1114, 1230 to 1284, 1347 and 1523 to 1592 cm^{-1}. Importantly no strong feature at 977 cm^{-1} was observed in the data, suggesting that this band is not the dominant discriminant within the patient samples, in contrast with the in-vitro study findings.

The corresponding PC score plots and loadings of Raman spectra recorded on both epithelia and stroma of OC patient tissues are shown in Figure 6. For the analysis on epithelial spectra the score plots of PC1 vs PC2 and PC2 vs PC3 are shown in Figures 6A,B, respectively. These plots show that the distribution of all scores strongly overlaps. The spectral loading vectors are also depicted in Figure 6C. Here, the PC1 loading vector appears to be the mean spectrum of epithelia, which describes 96.87% of explained variance of the studied dataset. The weaker spectral components are shown in loading vectors of PC 2 and 3 with 0.8 and 0.52% of variance, respectively.

Similar results were obtained for Raman spectra of stroma. Figure 6D,E respectively show the score plots of PC1 vs PC2 and PC2 vs PC3, where the distribution of all PC scores TRG strongly overlaps. The loading vector of PC1 (as in Figure 6F) accounts for 96.97% of the variance and resembles the mean spectrum of stroma. PC2 and 3 account for 0.73% and 0.48% of the variance, respectively. It is clear from this data that spectra from tissues with varying TRG score cannot be discriminated from one another using simple decomposition and visualisation.

This view is reaffirmed after visualisation of the IR spectra of OC tissue by TRG score. The mean pre-processed IR spectra of OC tissue at different TRG scores are plotted in Figure 7. Differences between each class of TRG score can be observed at the range of 1028 to 1148, 1148 to 1180 and 1270 to 1350 cm^{-1}.

The corresponding PC score plots and loadings of IR spectra are shown in Figure 8. The score plots of PC1 vs PC2 (Figure 8A) and PC2 vs PC3 (Figure 8B) demonstrate that the distribution of PC scores by TRG class strongly overlap. Figure 8C again represents the first three loading vectors where PC1 loading resembles the average spectrum of tissue and encapsulates 99.74% of the explained variance. PC 2 and 3 loading vectors describe far smaller proportions of variance with 0.12% and 0.05% of variance, respectively. Again, it is clear that FTIR spectra of OC tissues cannot be discriminated from one another in terms of TRG score using simple visualisation, implying that more complex classification algorithms are warranted.

3.3 | Classification of TRG score from OC tissue spectra

Several models of TRG score classification were constructed, with varying threshold between responders and non-responders. As mentioned earlier, TRG score varies from 1 to 5, with 1 signifying full pathological response and 5 signifying no response to neoCRT. However, within the intermediate classes with TRG 2 or 3 a partial response is seen, with some tumour debulking. Therefore, various hypotheses were tested within the models, which required the creation of several grouped sets from the spectral data:

i. In the first spectra from patients with TRG 1 were employed as the positive class (responders) and spectra from patients with TRG 2 to 5 as the negative class (non-responders). Here the objective is to test whether it is possible to spectrally discriminate between full responders and a mix of partially and unresponsive patients.
ii. Similarly in the second strategy patients with TRG 1 and 2 were grouped as the positive class (full responders and partial responders) with patients having TRG 3 to 5 (slight to no response) grouped as the negative class. Here the objective is to determine whether spectra of tissue can be used to classify full and partial responders from patients with slight to no response.
iii. In the final strategy patients with TRG 1 to 3 were grouped as the positive class (full, partial and slight response) while patients with TRG 4 to 5 (no response) were grouped the negative class. Here the objective is to determine whether spectra can be used to classify patients with a pathological response (regardless of level) vs those who exhibit no response to neoCRT.

Models classifying response class were implemented for both pre-processed Raman and IR spectra. The performance of each model was measured and evaluated with .632 bootstrap cross-validation (as described in section 2.5.2).

The optimal classification performance of pathological response using Raman spectra are shown in Table 2, with separate results for modelling with spectra of epithelia and stroma. For the Raman spectra of epithelia the optimal model was obtained with the PCA-QDA algorithm with the highest ROC AUC for the classification of TRG 1 vs 2 to 4 and TRG 1 to 2 to 3 vs 4 with 0.82 and 0.83, respectively. The optimal model for TRG 1 to 2 vs 3 to 4 classification was obtained with a KNN algorithm (ROC AUC of 0.73).

For the Raman spectra of stroma the KNN algorithm generated the optimal models for classifying TRG 1 to 2 vs 3 to 4 and TRG 1 to 2 to 3 vs 4 with ROC AUC's of 0.72 and 0.80 respectively. The highest AUC score of 0.85 was calculated for the PCA-QDA model in classifying TRG 1 vs 2 to 3 to 4.

Similarly the classification of neoCRT response with IR spectra are shown in Table 3, where the highest ROC AUC was obtained for the KNN model in discriminating TRG 1 vs 2 to 3 to 4 to 5 with 0.86, with 0.77 for TRG 1 to 2 vs 3 to 4 to 5. For the classification of TRG 1 to 2 to 3 vs 4 to 5, the PCA-QDA model provided an optimised AUC value of 0.81.

Among the three response classifications, the classification of TRG 1 to 2 vs 3 to 4(−5) models were the least accurate for both Raman and IR spectra. This implies that spectra from tissues with TRG 2 are more similar to tissues with TRG 3 to 4 to 5 than TRG 1.

Likewise, the grouping of TRG3 spectra with TRG1-2 results in high classification performance when classified vs spectra from the TRG4(−5) group. This may be due to the fact that spectra from patients with TRG 3 pathology are more similar to those with TRG 1 to 2 pathology, resulting in a discrimination against spectra from the TRG 4 to 5 pathology with a greater degree of accuracy.

Overall these results also suggest that spectra from tissues with TRG 1 are the most spectrally distinct (with a ROC AUC 0.82 in classifying TRG 1 vs 2 to 3 to 4(−5) using either Raman or IR spectra).

Current options for prediction of pCR within this space are unfortunately very limited, and none appear to be in routine clinical use. There is some evidence that diffusion weighted coefficients extracted from MRI during the radiotherapy portion of neo-adjuvant treatment are predictive of pCR.[44–46] Clearly this does not allow such knowledge to be used for individualization of treatment at planning. Results are yet to issue from the PRIDE trial[47] which is testing the predictive capacity of pre-operative MRI and 18 FDG PET here. Additionally pilot investigations of the utility of PET-CT[48] and CT[49] have

demonstrated reasonable performance in predicting pCR (accuracy of ~75% and ROC AUC of 0.71, respectively). Related work on proteomics of serum[50] and on MRI of locally advanced colorectal cancer[51] (in which the biology is similar to OC) provide the best benchmarking against which the present work might be compared. In the former study serum complement protein levels were found to be predictive of pCR with sensitivity and specificity of 78.6% and 83.3%, respectively. In the latter study a nomogram based on preoperative MRI of OC demonstrated a ROC AUC in the region of 0.82, which is remarkably similar to that delivered by our technology. In totality each of these technologies provide predictive performances similar to that presented here. This provides some context regarding the positioning of the current technology within the broader efforts to predict pCR prior to commencement of therapy.

4 | CONCLUSION

Pre-classification of therapy response before neo-adjuvant treatment remains a challenge for existing biological assays. The present study aimed to investigate whether vibrational spectra of OC tissue acquired prior to neoCRT might have predictive significance in identifying patients who receive a full, partial or no pathological response to neo-adjuvant therapy. Our results suggest that this may indeed be the case, where the evidence also suggests spectrally distinct classes within patients who receive a full pathological response (TRG 1), patients who have a partial response (TRG 2 and 3) and those where no response (TRG 4 and 5) is evident. While the explanatory power of the parallel in-vitro study on the OE33 P and OE33 R cell line model in the context of the overall study has yet to be elucidated, a spectral biomarker of radioresistance in this model was detected at 977 cm^{-1}. The molecular identity of this biomarker, and spectral biomarkers segregating patients on TRG score, remains to be elucidated.

ACKNOWLEDGMENTS

This work was financially supported by a Science Foundation Ireland Technology Innovation and Development Award (Grant number 12/TIDA/B2406; 2013-2015) and a Health Research Board Health Research Award (Grant number HRA-POR-2015-1314; 2015-2020) and was conducted at the SFI ADAPT Centre, TU Dublin. The ADAPT SFI Centre for Digital Media Technology is funded by Science Foundation Ireland through the SFI Research Centres Programme and is co-funded under the European Regional Development Fund (ERDF) through Grant # 13/RC/2106.

CONFLICT OF INTEREST

The authors declare no conflict of interest.

AUTHOR CONTRIBUTIONS

Aidan D. Meade and Jacintha O'Sullivan conceived of and obtained funding for the study. Adrian Maguire, Vicki Weldon and Naomi Jackson performed spectroscopic measurements while Catherine Mooney and Thi N. Q. Nguyen developed modelling approaches. John V. Reynolds, Narayanasamy Ravi and D. O'Toole provided OC tissues. Aoife A. Maguire performed pathological assessments of the tissues. John V. Reynolds and Niamh Lynam-Lennon provided clinical and experimental support and the use of the isogenic cell line model. Aidan D. Meade wrote the manuscript with Thi N. Q. Nguyen.

DATA AVAILABILITY STATEMENT

The data that support the findings of this study are available from the corresponding author upon reasonable request.

ORCID

Aidan D. Meade https://orcid.org/0000-0003-0353-9768

REFERENCES

[1] M. Arnold, I. Soerjomataram, J. Ferlay, D. Forman, *Gut* **2015**, *64*, 381.
[2] J. Offman, F. Pesola, P. Sasieni, *Br. J. Cancer.* **2018**, *118*, 1391.
[3] M. Arnold, M. Laversanne, L. M. Brown, S. S. Devesa, F. Bray, *Am. J. Gastroenterol.* **2017**, *112*(8), 1247.
[4] J. V. Reynolds, C. Muldoon, D. Hollywood, N. Ravi, S. Rowley, K. O'Byrne, J. Kennedy, T. J. Murphy, *Ann. Surg.* **2007**, *245*, 707.
[5] M. Berho, M. Oviedo, E. Stone, C. Chen, J. Nogueras, E. Weiss, D. Sands, S. Wexner, *Colorectal Dis.* **2009**, *11*, 254.
[6] D. Beddy, J. M. P. Hyland, D. C. Winter, C. Lim, A. White, M. Moriarty, J. Armstrong, D. Fennelly, D. Gibbons, K. Sheahan, *Ann. Surg. Oncol.* **2008**, *15*, 3471.
[7] L. J. van, t Veer, R. Bernards, *Nature* **2008**, *452*, 564.
[8] M. J. van de Vijver, D. He Yudong, L. J. van, t Veer, H. Dai, A. A. M. Hart, D. W. Voskuil, G. J. Schreiber, J. L. Peterse, C. Roberts, M. J. Marton, M. Parrish, D. Atsma, A. Witteveen, A. Glas, L. Delahaye, T. van der Velde, H. Bartelink, S. Rodenhuis, E. T. Rutgers, S. H. Friend, R. Bernards, *N. Engl. J Med.* **2002**, *347*, 1999.
[9] R. Rosell, T. G. Bivona, N. Karachaliou, *Lancet* **2013**, *382*, 720.
[10] J. A. Ludwig, J. N. Weinstein, *Nat. Rev. Cancer* **2005**, *5*, 845.
[11] I. I. Wistuba, J. G. Gelovani, J. J. Jacoby, S. E. Davis, R. S. Herbst, *Nat. Rev. Clin. Oncol.* **2011**, *8*, 135.
[12] B. Haibe-Kains, N. El-Hachem, N. J. Birkbak, A. C. Jin, A. H. Beck, H. J. W. L. Aerts, J. Quackenbush, *Nature* **2013**, *504*, 389.

[13] F. Huber, M. Montani, T. Sulser, R. Jaggi, P. Wild, H. Moch, H. Gevensleben, M. Schmid, S. Wyder, G. Kristiansen, *British J. Cancer.* **2015**, *112*, 140.
[14] M. Diem, A. Mazur, K. Lenau, J. Schubert, B. Bird, M. Miljkovic, C. Krafft, J. Popp, *J. Biophoton.* **2013**, *6*, 855.
[15] C. L. Zavaleta, E. Garai, J. T. C. Liu, S. Sensarn, M. J. Mandella, D. V. d. Sompel, S. Friedland, J. V. Dam, C. H. Contag, S. S. Gambhir, *PNAS* **2013**, *110*, E2288.
[16] D. O'Dea, M. Bongiovanni, G. P. Sykiotis, P. G. Ziros, A. D. Meade, F. M. Lyng, A. Malkin, *Cytopathology* **2019**, *30*, 51.
[17] I. R. Ramos, A. D. Meade, O. Ibrahim, H. J. Byrne, M. McMenamin, M. McKenna, A. Malkin, F. M. Lyng, *Faraday Discuss.* **2016**, *187*, 187.
[18] S. Mittal, K. Yeh, L. S. Leslie, S. Kenkel, A. Kajdacsy-Balla, R. Bhargava, *Proc. Natl. Acad. Sci. U S A.* **2018**, *115*, E5651.
[19] F. M. Lyng, D. Traynor, T. N. Q. Nguyen, A. D. Meade, F. Rakib, R. Al-Saady, E. Goormaghtigh, K. Al-Saad, M. H. Ali, *PLoS One* **2019**, *14*, e0212376.
[20] H. J. Butler, P. M. Brennan, J. M. Cameron, D. Finlayson, M. G. Hegarty, M. D. Jenkinson, D. S. Palmer, B. R. Smith, M. J. Baker, *Nat. Commun.* **2019**, *10*, 4501.
[21] C. Hughes, G. Clemens, B. Bird, T. Dawson, K. M. Ashton, M. D. Jenkinson, A. Brodbelt, M. Weida, E. Fotheringham, M. Barre, J. Rowlette, M. J. Baker, *Sci. Rep.* **2016**, *6*, 1–8.
[22] A. D. Meade, A. Maguire, J. Bryant, D. Cullen, D. Medipally, L. White, B. McClean, L. Shields, J. Armstrong, M. Dunne, E. Noone, S. Bradshaw, M. Finn, A. M. Shannon, O. Howe, F. M. Lyng, *Int. J. Radiat. Biol.* **2019**, *95*, 44.
[23] A. D. Meade, O. Howe, V. Unterreiner, G. D. Sockalingum, H. J. Byrne, F. M. Lyng, *Faraday Discuss.* **2016**, *187*, 213.
[24] A. Maguire, I. Vegacarrascal, L. White, B. McClean, O. Howe, F. M. Lyng, A. D. Meade, *Radiat. Res.* **2015**, *183*, 407.
[25] H. Nawaz, F. Bonnier, P. Knief, O. Howe, F. M. Lyng, A. D. Meade, H. J. Byrne, *Analyst* **2010**, *135*, 3070.
[26] D. K. R. Medipally, T. N. Q. Nguyen, J. Bryant, V. Untereiner, G. D. Sockalingum, D. Cullen, E. Noone, S. Bradshaw, M. Finn, M. Dunne, A. M. Shannon, J. Armstrong, F. M. Lyng, A. D. Meade, *Cancers (Basel)* **2019**, *11*, 925–943.
[27] D. Cullen, J. Bryant, A. Maguire, D. Medipally, B. McClean, L. Shields, E. Noone, S. Bradshaw, M. Finn, M. Dunne, A. M. Shannon, J. Armstrong, O. Howe, A. D. Meade, F. M. Lyng, *Transl. Biophoton.* **2020**, e201900035. https://doi.org/10.1002/tbio.201900035.
[28] A. Mandard, F. Dalibard, J. Mandard, J. Marnay, M. Henry-Amar, J. Petiot, A. Roussel, J. Jacob, P. Segol, G. Samama, *Cancer* **1994**, *73*, 2680–2686.
[29] N. Lynam-Lennon, J. V. Reynolds, G. P. Pidgeon, J. Lysaght, L. Marignol, S. G. Maher, *Radiat. Res.* **2010**, *174*, 703.
[30] N. Lynam-Lennon, S. G. Maher, A. Maguire, J. Phelan, C. Muldoon, J. V. Reynolds, J. O'Sullivan, *PLoS One.* **2014**, *9*, e100738.
[31] N. Lynam-Lennon, J. V. Reynolds, L. Marignol, O. M. Sheils, G. P. Pidgeon, S. G. Maher, *J. Mol. Med. (Berl).* **2012**, *90*, 1449.
[32] E. O. Faolain, M. B. Hunter, J. M. Byrne, P. Kelehan, H. A. Lambkin, H. J. Byrne, F. M. Lyng, *J Histochem. Cytochem.* **2005**, *53*, 121.
[33] D. K. Medipally, A. Maguire, J. Bryant, J. Armstrong, M. Dunne, M. Finn, F. M. Lyng, A. D. Meade, *Analyst* **2017**, *142*, 1216.
[34] P. Bassan, A. Sachdeva, A. Kohler, C. Hughes, A. Henderson, J. Boyle, J. H. Shanks, M. Brown, N. W. Clarke, P. Gardner, *Analyst* **2012**, *137*, 1370.
[35] S. Wold, K. Esbensen, P. Geladi, *Chemom. Intell. Lab. Syst.* **1987**, *2*, 37.
[36] E. Fix, J. L. Hodges, *Discriminatory Analysis, Vol.*, Randolph Field, Texas **1951**.
[37] R. O. Duda, P. E. Hart, *Pattern Classification and Scene Analysis*, Wiley, **1973**.
[38] J. D. Knoke, *Biometrics* **1982**, *38*, 191.
[39] R. G. Brereton, G. R. Lloyd, *J. Chem.* **2014**, *28*, 213.
[40] P. S. Gromski, H. Muhamadali, D. I. Ellis, Y. Xu, E. Correa, M. L. Turner, R. Goodacre, *Anal. Chim. Acta.* **2015**, *879*, 10.
[41] J. A. Westerhuis, H. C. J. Hoefsloot, S. Smit, D. J. Vis, A. K. Smilde, E. J. J. v. Velzen, J. P. M. v. Duijnhoven, F. A. v. Dorsten, *Metabolomics* **2008**, *4*, 81.
[42] R. J. Tibshirani, B. Efron, *An Introduction to the Bootstrap*, **1993**.
[43] B. Efron, *J. Am. Stat. Assoc.* **1983**, *78*, 316.
[44] S. Heethuis, L. Goense, P. van Rossum, A. Borggreve, S. Mook, F. Voncken, A. Bartels-Rutten, B. Aleman, R. van Hillegersberg, J. Ruurda, G. Meijer, J. Lagendijk, A. van Lier, *Acta Oncol.* **2018**, *57*, 1201.
[45] P. van Rossum, A. van Lier, M. van Vulpen, O. Reerink, J. Lagendijk, S. Lin, R. van Hillegersberg, J. Ruurda, G. Meijer, I. Lips, *Radiother. Oncol.* **2015**, *115*, 163.
[46] A. Borggreve, L. Goense, P. van Rossum, S. Heethuis, R. van Hillegersberg, J. Lagendijk, M. Lam, A. van Lier, S. Mook, J. Ruurda, M. van Vulpen, F. Voncken, B. Aleman, A. Bartels-Rutten, J. Ma, P. Fang, B. Musall, S. Lin, G. Meijer, *Int. J. Radiat. Oncol. Biol. Phys.* **2020**, *106*, 998.
[47] A. Borggreve, S. Mook, M. Verheij, V. Mul, J. Bergman, A. Bartels-Rutten, L. Ter Beek, R. Beets-Tan, R. Bennink, M. van Berge Henegouwen, L. Brosens, I. Defize, J. van Dieren, H. Dijkstra, R. van Hillegersberg, M. Hulshof, H. van Laarhoven, M. Lam, A. van Lier, C. Muijs, W. Nagengast, A. Nederveen, W. Noordzij, J. Plukker, P. van Rossum, J. Ruurda, J. van Sandick, B. Weusten, F. Voncken, D. Yakar, G. Meijer, *BMC Cancer* **2018**, *18*.
[48] M. W. Macomber, A. Samareh, W. A. Chaovalitwongse, S. R. Bowen, S. A. Patel, J. Zeng, M. Nyflot, *Int. J. Radiat. Oncol. Biol. Phys.* **2016**, *96*, E699.
[49] Z. Yang, B. He, X. Zhuang, X. Gao, D. Wang, M. Li, Z. Lin, R. Luo, *J. Radiat. Res.* **2019**, *60*, 538.
[50] S. Maher, D. McDowell, B. Collins, C. Muldoon, W. Gallagher, J. Reynolds, *Ann. Surg.* **2011**, *254*, 809.
[51] X. Tang, W. Jiang, H. Li, F. Xie, A. Dong, L. Liu, L. Li, *Radiother. Oncol.* **2020**, *148*, 97.

SUPPORTING INFORMATION

Additional supporting information may be found online in the Supporting Information section at the end of this article.

How to cite this article: Nguyen TNQ, Maguire A, Mooney C, et al. Prediction of pathological response to neo-adjuvant chemoradiotherapy for oesophageal cancer using vibrational spectroscopy. *Translational Biophotonics*. 2020;e202000014. https://doi.org/10.1002/tbio.202000014